NaI:Tl response to relativistic Ne, Ar, and Fe ions

M. H. Salamon* and S. P. Ahlen
Department of Physics and Space Sciences Laboratory, University of California, Berkeley, California 94720
(Received 16 December 1980; revised manuscript received 8 June 1981)

Data are presented on the response of thallium-activated sodium iodide to relativistic ^{20}Ne, ^{40}Ar, and ^{56}Fe ions in the energy interval 0–550 MeV/amu. The resulting scintillation efficiency curves are found to rise with decreasing stopping power, contrary to conclusions drawn from lower-energy heavy-ion data. A scintillation model is developed which provides an excellent qualitative fit to data spanning two orders of magnitude in stopping power and which demonstrates *a posteriori* the failure of the activator depletion mechanism for saturation. This model includes a calculation of the prompt dose profile, the diffusion of excitons resulting from the deposited energy, and a second-order annihilation process which accounts for the observed saturation.

I. INTRODUCTION

Previous studies of the scintillation of alkali halide crystals have been limited to the use of singly charged particle beams of various energies and to heavy-ion beams with energies less than 10 MeV/amu.[1–9] In this paper we report data which extend the heavy-ion measurements up to 550 MeV/amu. These data are of interest for two reasons: (1) The spatial distribution of deposited energy for relativistic ions is considerably different than for slower ions with the same stopping power; since ionization quenching processes are dependent on energy density, it is of intrinsic physical interest to examine the difference of alkali halide repsonse to these different types of ions; (2) successful applications of alkali halide scintillators to problems involving relativistic heavy ions in astrophysics and nuclear physics require accurate calibrations of detector response; to date no such calibrations have been available.

The data presented in this paper were obtained with a thallium-doped (0.0013 mole fraction) sodium iodide crystal [NaI(Tl)] exposed to relativistic ^{20}Ne, ^{40}Ar, and ^{56}Fe beams from the Lawrence Berkeley Laboratory's Bevalac. More details of the experimental configuration and of the analysis techniques will be given in later sections. Results of both pure and applied physical interest will be presented. Of particular physical interest is the fact that by taking into account the spatial distribution and diffusion of energy in the wake of a heavy ion, the observed saturation of scintillation in NaI(Tl) can be accounted for by assuming the existence of a second-order annihilation process with a rate constant determined from the data. This model is attractive in that it provides a good fit to data for ions ranging in stopping power from 10 to 5000 MeV $cm^2 g^{-1}$ and in atomic number from 1 to 26. The results of the calculations for this model also demonstrate *a posteriori* the failure of the activator depletion hypothesis to account for alkali halide saturation, a fact observed experimentally[3,10] but which previously lacked an explanation. For purposes of practical implementation of NaI(Tl) scintillators, we have found that a parameter used to group alkali halide data at low energies[11] seems to apply to our high-energy data as well. This should be of use to those using sodium iodide scintillators in previously uncharted territory.

II. HEAVY-ION DATA

A. Experimental configuration

The experiment was conducted at LBL's Bevalac, during which several types of scintillators (mostly organic plastic and liquid), including a standard Harshaw Chemical Co. NaI:Tl crystal (6.35 cm diam × 1.27 cm thick, type *D* housing), were examined. In three separate runs, spaced 48 h apart, ^{20}Ne, ^{40}Ar, and ^{56}Fe ions beams of fixed energy ($\sim$600 MeV/amu) were directed onto the experimental apparatus shown in Fig. 1. Passage through an automated absorber consisting of eight extremely precise plates of thickness $2^n (n = 1, \ldots, 8)$, made mostly of a high-Z material (Pb) to minimize nuclear interactions during slowing, allowed us rapidly and nearly continuously to vary the ion energy entering the NaI:Tl crystal. A silicon semiconductor detector situated midstream discriminated against ions having undergone charge-changing nuclear interactions in the absorber. The NaI:Tl crystal, all but one face covered by an Al-Al_2O_3 housing, illuminated the interior of a light diffusion box. The interior of the light diffusion box was painted with a highly reflec-

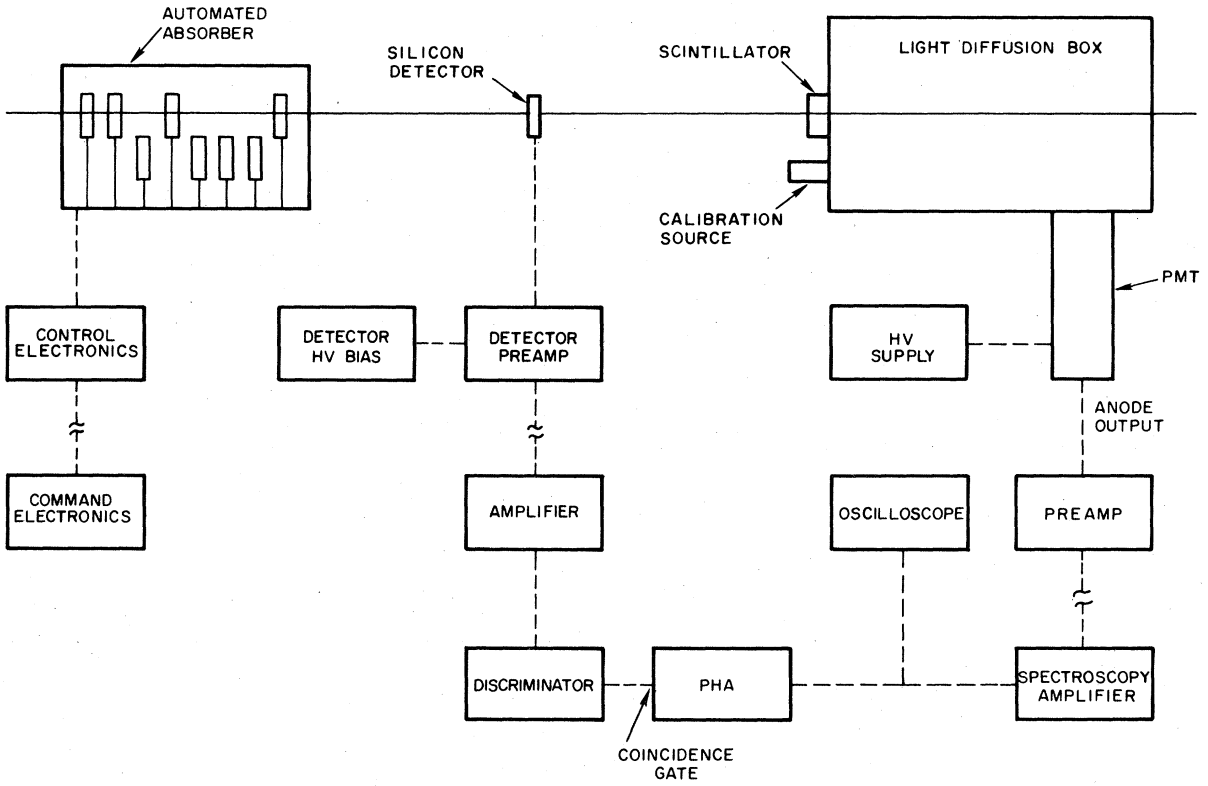

FIG. 1. Experimental configuration for Bevalac heavy-ion exposures.

tant, nearly wavelength-independent powder, $BaSO_4$.[12,13] Light entering through a window (to which was attached the scintillator) was randomized through successive "bounces" during which original spatial information was lost. The constant fraction of the total light collected by the single photomultiplier tube (PMT) was, therefore, nearly independent of the ion entry position at the scintillator face (much less than 1% by computer calculation[14]). Use of a light diffusion box also enabled us rapidly and reproducibly to change scintillator samples with assurance of a constant scintillator-PMT coupling efficiency.

The PMT used was an EMI9817Q tube with an S-20 (trialkali) photocathode and a fused quartz window. To calibrate against tube gain drifts occurring during the course of the exposures, a calibration source of ^{241}Am-doped NaI:Tl with an activity of ~ 3 nCi was prepared for us by Harshaw Chemical Co. The 5.49-MeV α's emitted within this calibration crystal provided a constant light level that was adopted as the unit of light output; all signals are given in units of this source. Because of the temperature dependence of NaI response, the temperature was controlled so as to limit response variations to $\lesssim 0.4\%$ over the three exposures. Tests of PMT linearity were made and slight nonlinearity at high signal strengths were corrected for. (Full analysis details are given elsewhere.[15])

B. Method of analysis of heavy-ion data

The most probable pulse height of each pulse height spectrum (consisting of $\sim 10^4$–10^5 individual ion pulses) was read to ~ 1–2 channel accuracy; afterwards these channel numbers were converted to give light outputs ΔL in units of our calibration source signal. To determine the total energy ΔE deposited in the scintillator (throughout, a script E denotes total energy with units of MeV; a captial E denotes energy in units of MeV/amu), the ion energy upon entering (E_i) and leaving (E_0) the crystal had to be calculated. Assuming a known beam energy E_{top}, at the top of the experimental apparatus, a range-energy program integrated the energy loss through all the tabulated upstream matter in the beam line (including any absorber plate mass) to arrive at values for E_i and E_0. The range-energy program[16] used in this procedure incorporated higher order corrections in Z_1 to stopping power[17] to provide an energy accuracy[18] of ~ 0.5–1.0% for the charges and energies used. Since the beam extraction energy from the accelerator was not known precisely, E_{top} was treated as a floating parameter which was fixed for each charge with excellent consistency during the data-fitting procedure described below.

Figures 2(a)–2(c) show the "raw" response for Ne, Ar, and Fe. The cusp in each figure occurs at an

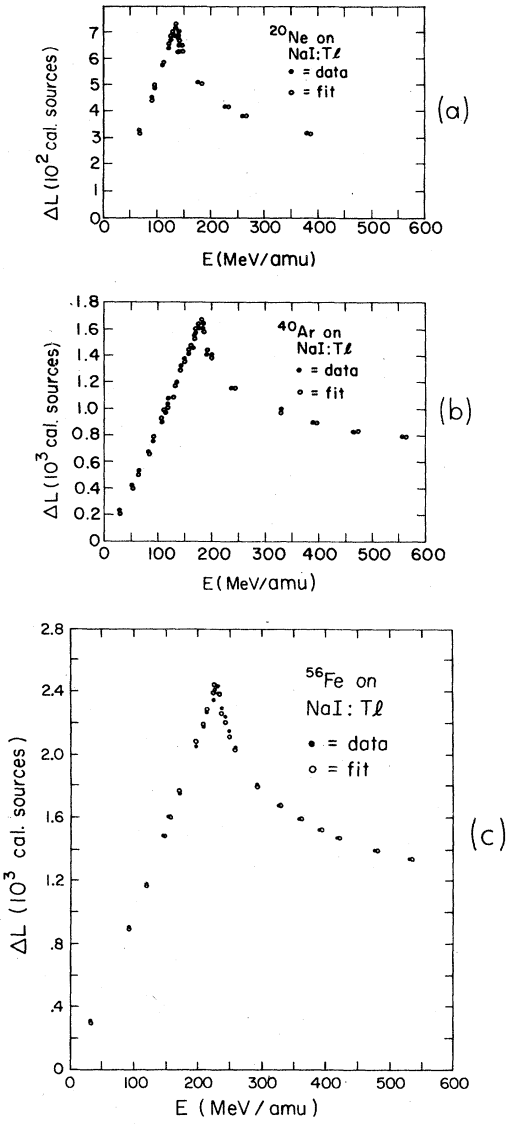

FIG. 2. "Raw" light response curves for ^{20}Na (a), ^{40}Ar (b), and ^{56}Fe (c). Ordinate values are proportional to measured signals, and abscissa values are calculated using the fitting method described in text. Excellent agreement between data (●) and fit (○) is evident. In this and subsequent figures, the unit "calibration source" is abbreviated as "cal source."

energy where the particle is stopped just at the exit face of the crystal (maximum energy deposition). To fit the data, the light response L of an *infinitely* thick crystal was taken to have the form

$$L = \sum_{k=1}^{n} a_k E_i^k \ .$$

Thus, for an ion entering a finitely thick crystal with energy E_i and exciting with energy E_0, the light

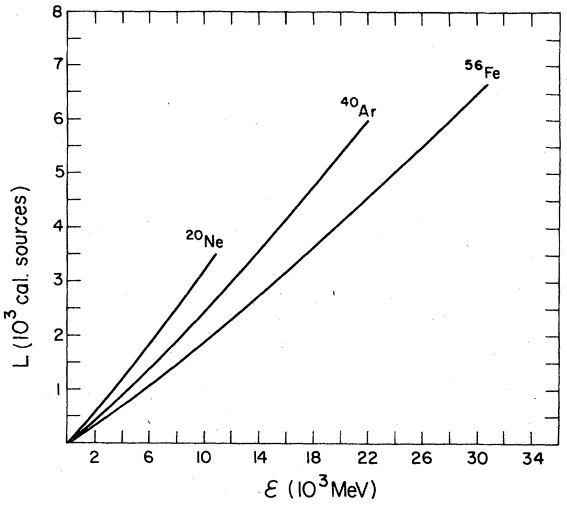

FIG. 3. $L(\mathcal{E})$ polynomial curves for ^{20}Ne, ^{40}Ar, and ^{56}Fe.

response is

$$\Delta L(E_i) = L(E_i) - L(E_0) = \sum_{k=1}^{n} a_k (E_i^k - E_0^k) \ .$$

Use of a least-squares technique then determined the coefficients a_k for a given polynomial order n.

The resulting fits to the data are also shown in Figs. 2(a)–2(c). Once $L(E)$ is known (Fig. 3), the scintillation efficiency (units of cal source/MeV) fol-

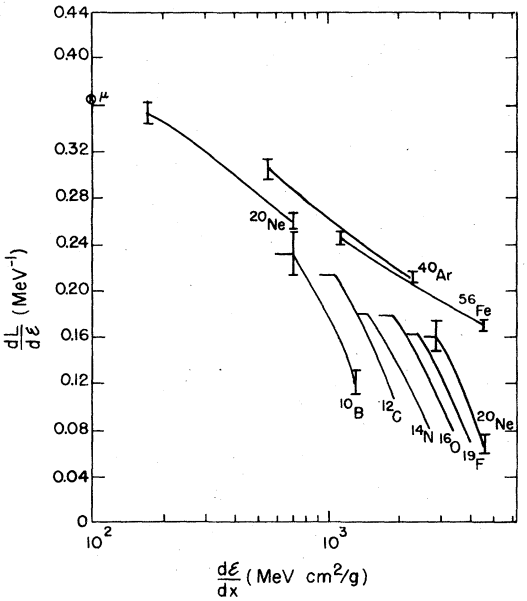

FIG. 4. Scintillation efficiency curves ($dL/d\mathcal{E}$ vs $d\mathcal{E}/dx$) for both relativistic heavy-ion data and low-energy heavy-ion data Ref. 1). The error bars on the low-energy data represent uncertainties in the cross-calibration procedure. Error bars on relativistic ion data represent experimental erros. Measurement of the muon point (μ) is discussed in Ref. 15.

lows immediately, $dL/d\mathcal{E} = (1/A_1)\,dL/dE$ (A_1 being the atomic weight of the ion in amu). These are shown in Fig. 4. Since $L(E)$ is differentiated to provide the quantity of interest, the choice of polynomical order n is important. Figure 5(a) shows $dL/d\mathcal{E}$ vs E calculated for ^{56}Fe on NE110, a commercial plastic scintillator, where the polynomial order varies from 3 to 7. As seen, there is practically no sensitivity to n in the region $50 \leq E \leq 500$ MeV/amu, so the validity of our $dL/d\mathcal{E}$ values is assumed to be confined to this energy interval. Figure 5(b) shows χ^2 vs n; $n = 5$ was chosen as optimal. To estimate the influence of measurement error on $dL/d\mathcal{E}$, raw Fe data were augmented by a normal distribution of random numbers whose σ was comparable to the estimated error. The resulting variation in $dL/d\mathcal{E}$ was of the order of 1%, which when added to other sources of error gives an estimated total of $\sim 2.5\%$.

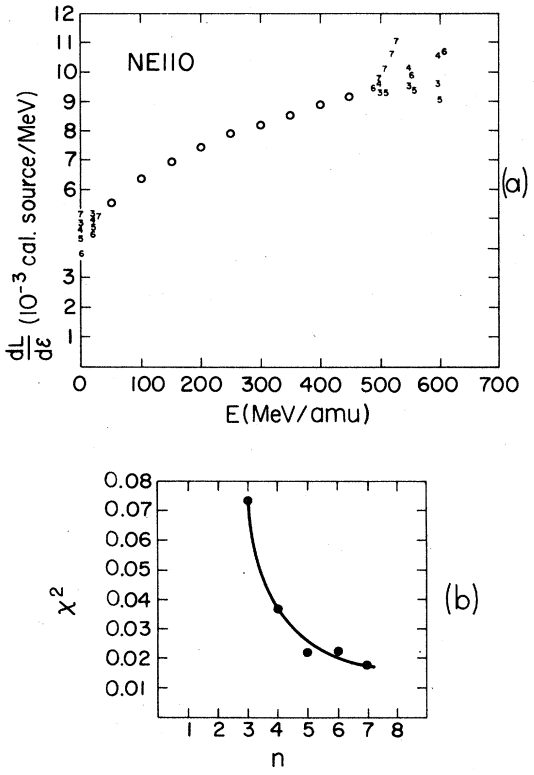

FIG. 5. (a) $dL/d\mathcal{E}$ calculated from $L(E)$ for NE110, a commerical plastic scintillator, where $L(E)$ is a fitted polynomial of order $n = 3$ to 7. Insensitivity to polynomial order is demonstrated for $50 < E < 500$ MeV/amu (open circles). (b) Least-squares χ^2 vs polynomial order n, from which $n = 5$ was chosen as optimal. The anomalous *increase* in χ^2 at $n = 6$ is most likely due to onset of computational illcondition.

C. Comparison with other data

Shown along with our data in Fig. 4 is the extensive low energy (1–10 MeV/amu) heavy-ion data of Newman and Steigert (NS).[1] A salient feature of both sets of data is the separation of the efficiency curves for each charge; for a given stopping power, the larger charge has the higher efficiency. This is unequivocal evidence for the important role the distribution of dose energy in the lattice plays in scintillation response; regions of higher energy density have a reduced efficiency due to ionization quenching. Lower velocity particles tend to deposit more energy in the track "core" a high-energy density region immediately about the projectile trajectory, than do higher velocity particles which produce greater numbers of high-energy secondary electrons (δ rays) which transport energy to regions of low-energy density. Since $d\mathcal{E}/dx$ is nearly proportional to Z_1^2/β^2 (β being the ion velocity of units of c), for a fixed $d\mathcal{E}/dx$ value a higher Z_1 particle is expected to have a higher efficiency. The role of ionization quenching is corroborated in Fig. 6. Here our $dL/d\mathcal{E}$ data for Ne, Ar, and Fe are shown versus E, or equivalently, velocity. For a given velocity, the dose profile is roughly independent of charge, apart from an overall factor of Z_1^2. The unambiguous drop in average efficiency with increase in Z_1 attests to the enhanced role of ionization quenching due to this Z_1^2 factor in the dose profile. It should be pointed out that although the relativistic Ar curve as shown in Fig. 4 lies *above* the Fe curve, this separation is not significant, being within estimated errors; in fact, the separation should be in the other direction.

To cross-calibrate our data with those of NS, we made use of parametrization by Womack *et al.*[11]

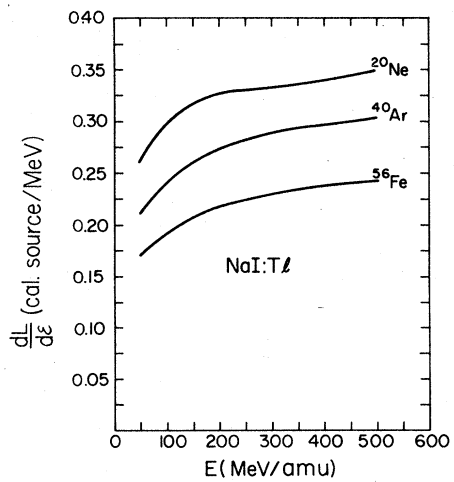

FIG. 6. Scintillation efficiency $dL/d\mathcal{E}$ of relativistic ^{20}Ne, ^{40}Ar, and ^{56}Fe as function of energy E (MeV/amu).

They noticed that nearly all the data of NS for $Z_1 \geq 2$ fall on a single straight line when expressed as L vs $\epsilon \propto \beta_0^3 A_1 / Z_1^{2/3}$, β_0 being the velocity of the ion entering the (infinitely thick) crystal. (A similar relation was found for CsI:Tl data.[19]) We have found that this relationship is maintained with our data as well, with the relativistic Ne, Ar, and Fe data nearly falling on a common straight line. By assuming that a single line fits both sets of data as shown in Fig. 7, a calibration factor is determined that connects both sets of data. The validity of this procedure is seemingly confirmed by the resultant smooth "joining" of the two ^{20}Ne curve segments in Fig. 4. That this linear parametrization, which takes no ostensible account of track structure, holds for all charges over three orders of magnitude light output is quite remarkable and provocative. Being unable to explain its apparent success, we merely emphasize its potential use to experimentalists while issuing the caveat that its possible utility is based on limited data.

A prominent feature of the original NS heavy-ion data is the near discontinuity of slope of each ion's efficiency curve at ~ 7 MeV/amu, where a constant, plateau value is reached as indicated in Fig. 4. The relativistic data indicate that the ion efficiencies in fact do not level off, but continue to rise with a gentler slope as $d\mathcal{E}/dx$ decreases. That a sudden shift in efficiency slope occurs at this velocity for all charges, however, is corroborated by Blue and Liu,[3] who measured proton and alpha efficiencies in unactivated (77 and 300 K) and activated (77 K) LiI, NaI, KI, RbI, and CsI. In all but one case they observed an abrupt discontinuity in α efficiency at ~ 6 MeV/amu. They concluded that since this phenomenon was independent of activator concentration, temperature, and even alkali type, it involved a velocity effect involving the iodine atom.

Figure 8 combines additional NaI:Tl response data to give a broader picture of NaI:Tl behavior. Measurements by Eby and Jentschke[2] with protons (○) and α's (●) show protons to have a constant efficiency, while α efficiency begins to drop from the proton $dL/d\mathcal{E}$ value for $\mathcal{E} \lesssim 20$ MeV. While several other experiments collectively indicate a constant proton efficiency over the energy interval 60 keV–100 MeV by virtue of their proton L vs $\mathcal{E}$ points falling on a straight line passing through the origin (a positive energy offset indicates low-energy saturation), they do not all overlap or assure in any other way a common absolute scintillation efficiency. Therefore, the graphical placement of all proton points on a single $dL/d\mathcal{E}$ value in Fig. 8 should be viewed cautiously. Additional skepticism is due because, as shown, low-energy protons have a higher efficiency than α's of the same stopping power, in direct contradiction to all scintillation models incorporating track structure effects. Perhaps the strongest evidence against constant proton $dL/d\mathcal{E}$ is the careful experiment of Gwin and Murray[10] where proton efficiency was found to be nonlinear in CsI:Tl (short dash–long dash line in Fig. 8).

The combined heavy-ion data are normalized with

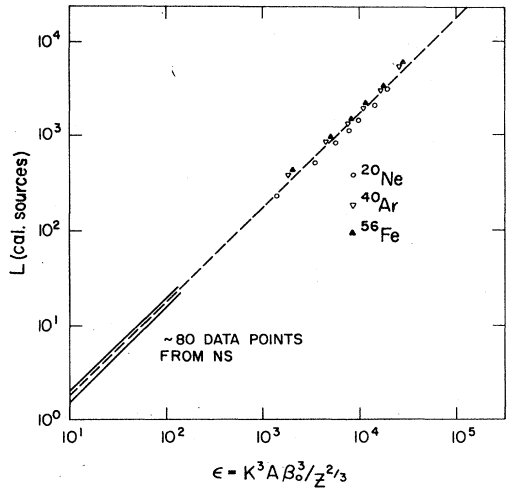

FIG. 7. Total light output L vs $\epsilon = K^3 A \beta_0^3 / Z^{2/3}$, where Z,A = ion atomic number and weight (in amu), β_0 is the entering velocity of the ion (in units of c), and K is the constant $(\frac{1}{2} m_u c^2)^{1/2}$, $m_u = 931.5$ MeV/c^2, The NS data fall within the band as shown.

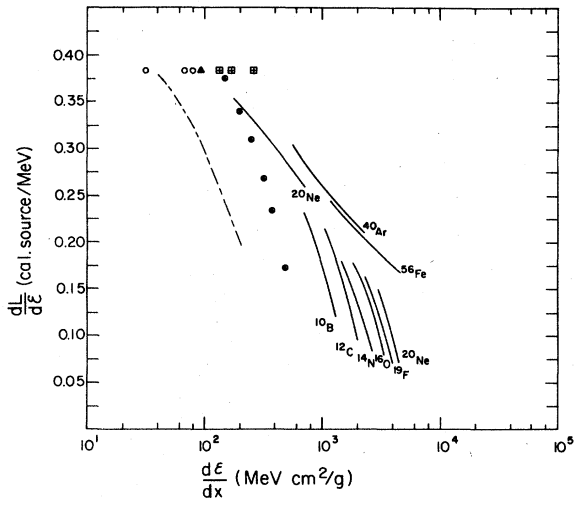

FIG. 8. Collected NaI:Tl scintillation efficiency ($dL/d\mathcal{E}$) data vs stopping power ($d\mathcal{E}/dx$) for various particles. Sources of these data are Ref. 1, low-energy heavy-ion curves (solid lines), α's (▲); Ref. 3, protons (○) and α's (●); Ref. 4, protons (open square with plus sign). Scintillation efficiency of CsI:Tl for protons is also shown (short-long dash, Ref. 10).

respect to protons by use of an α point (▲) of NS whose energy $\mathcal{E} = 40$ MeV places it at maximum (proton) efficiency according to the results of Eby and Jentschke[2] and Blue and Liu.[3] On the whole, the $Z_1 \geq 2$ data suggest that not only do α's attain proton efficiency at low enough $d\mathcal{E}/dx$, but also heavier ions do as well. The relativistic ^{20}Ne curve nearly reaches proton efficiency, and the ^{40}Ar and ^{56}Fe curves show no indication of not doing so (or coming as close as possible before minimum ionization energy is reached). A complete set of heavy-ion scintillation efficiency curves then quite likely appears as a fairly tight band of lines departing from maximum (proton) efficiency with gentle slope, with each ion then breaking away at ~ 6–7 MeV/amu into a steeper drop in efficiency with $d\mathcal{E}/dX$.

III. BASIC PROCESS IN ALKALI HALIDE SCINTILLATION

The physical mechanisms involved with pure and activated alkali halide (AH) scintillation are reviewed in detail elsewhere.[20–24] Briefly, when NaI is excited by high-energy charged particles or by photons, electron-hole (e-h) pairs are produced across a band gap of ~ 5.8 eV. For charged particle excitation, it takes approximately 20 eV of deposited energy on the average to produce one e-h pair. Recombination of the e-h pair within the *pure* lattice results in fluorescence at low temperatures. This process occurs in steps: within 10^{-13}–10^{-12} sec (Ref. 25) a hole is "self-trapped" in the lattice by dropping into a level a few eV above the valence band to form a "V_K center." This type of center was determined by ESR studies[26] to be a hole locally shared by two adjacent halogen ions, forming a molecular ion. Polarization studies[27] showed that V_K centers migrate by hopping across an activation barrier to neighboring halogen pair sites, resulting in a dramatic decrease in diffusion coefficient ($\sim 10^{-5}$ cm^2/sec for V_K centers compared to $\sim 10^{-1}$ cm^2/sec for free holes). Eventual recombination with a conduction-band electron forms a "self-trapped exciton" (STE) similar to a Frenkel exciton. From this state radiative decay occurs at low temperatures. At higher temperatures (e.g., 300 K) nonradiative decay processes[28] dominate and severely reduce luminescence,[29] making pure AH's very poor scintillators at room temperature.

Doping the crystal with an activator such at Tl dramatically enhances room-temperature luminescence since it acts as a trap for both electrons[26,30] and holes or V_K centers,[24] thereby severely curtailing the STE formation channel which provides essentially no luminescence. Trapping of e or h at a Tl site causes a change from the original $+1$ charge state of Tl in the NaI crystal: $e + \mathrm{Tl}^+ \rightarrow \mathrm{Tl}^0$, and $h + \mathrm{Tl}^+ \rightarrow \mathrm{Tl}^{2+}$. Most electrons, with their large diffusion coefficient of ~ 0.3 cm^2/sec,[22] quickly trap via $e + \mathrm{Tl}^+ \rightarrow \mathrm{Tl}^0$. Since holes rapidly self-trap in the lattice, only a small fraction "promptly" trap[23,24] via $h + \mathrm{Tl}^+ \rightarrow \mathrm{Tl}^{2+}$ while the remainder slowly diffuse as V_K centers, eventually trapping via $V_K + \mathrm{Tl}^+ \rightarrow \mathrm{Tl}^{2+}$ *or* $V_K + \mathrm{Tl}^0 \rightarrow \mathrm{Tl}^+ + h\nu$.[31] The latter process, resulting in characteristic fluorescence, has been shown to be an important contributor to the scintillation process.[23,32] The second process which contributes to fluorescence is $e + \mathrm{Tl}^{2+} \rightarrow \mathrm{Tl}^{+*} \rightarrow \mathrm{Tl}^+ + h\nu$, where Tl^{+*} is the excited state of Tl^+ (with decay time[33] ~ 0.22 μsec). Unlike holes which are deeply trapped in Tl^{2+} ions and do not escape thereafter, electrons are rather shallowly trapped in Tl^0 ions and do escape into the conduction band with significant frequency above a certain temperature. From there, they either retrap ($e + \mathrm{Tl}^+ \rightarrow \mathrm{Tl}^0$) or combine with Tl^{2+}, leading to radiative decay. This process continues until all electrons and holes have recombined, completing the scintillation process.

At high values of $d\mathcal{E}/dx$, "saturation," i.e., a drop in scintillation efficiency, occurs (Fig. 8). Various mechanisms have been proposed to explain this decline. Some models invoke depletion of activator sites as being responsible[34–36]: as the e-h pair density increases, the crystal's supply of unoccupied Tl sites becomes exhausted, and the remnant e-h pair density cannot contribute to scintillation for lack of available Tl sites. Though highly plausible, this mechanism has been convincingly disproved by the work of Gwin and Murray[10] and Blue and Liu[3]; apparently saturation is a property of the pure lattice only. Other models attribute scintillation efficiency decline to "ionization quenching"[37–39]: in regions of high-energy density (or equivalently, by assumption, high e-h pair density n), certain (unknown) nonradiative decay channels become efficient and depopulate much of the electronic excitation. Several plausible mechanisms resulting in enhanced loss of e-h pairs in regions of high pair density have been proposed and can be collectively accounted for by postulating a second-order (bimolecular, or n^2) nonradiative decay channel in the decay equation for dn/dt. Powell and Harrah[40] attribute saturation in pure polyvinyltoluence to an annihilative exciton-exciton interaction, in which two migrating lower energy excitons combine to form a single highly excited exciton which then rapidly and nonradiatively decays to a single lower energy exciton. Tolstoi and Abramov[41] consider a variety of crystals, both pure and activated, and find their collected scintillation efficiency versus energy-loss curves to be well described by a decay equation whose sole nonlinear term is $\propto n^2$. In the antiferromagnetic crystal $KMnF_3$, time-resolved spectroscopy of exciton emission confirmed the existence of a nonradiative second-order decay channel, indicating an annihilative exciton-exciton process.[42] In our model of alkali halide response we employ a

second-order decay channel to account for saturation; however, this does not uniquely specify the mode of interaction. Besides direct exciton-exciton (or pair-pair) interactions, other mechanisms which are governed by an n^2 rate include destruction of e-h pairs at excited activator sites,[40,41] and reabsorption of fluorescence photons at any of the many transiently excited chemcial species within the scintillator.[40] These latter two assume a linear relationship between energy dose and, respectively, excited activator concentration and fluorescent photon emission; these conditions are not always met for high-energy doses.

Following the results of Refs. 3 and 10, we deny the activator depletion hypothesis and adopt a second-order (n^2) quenching (nonradiative) decay channel. Although it may not by physically correct, it is mathematically equivalent and conceptually convenient to think of the quenching mechanism as being an annihilative exciton-exciton (or e-h pair$-e$-h pair) interaction.

An inescapable conclusion that comes with rejection of the activator depletion hypothesis is that two or more e-h pairs cannot indefinitely coexist within the effective capture volume of a Tl^+ ion. Were this possible, one e-h pair would occupy the Tl site, leaving the others ineffective with respect to luminescence; this, however, is simply a restatement of the activator depletion mechanism. Instead, an annihilation process must effectively reduce the e-h pair density below a level whose upper limit is provided by the inverse of the Tl^+ effective capture volume. This capture volume can be roughly estimated using experimental data on light output L for γ rays (low $d\mathcal{E}/dx$) vs Tl concentration[43] which has been found to fit a theoretical expression by Johnson and Williams[44] for scintillation efficiency versus Tl concentration. A nearly identical expression can be achieved with a model in which we assume each activator site to have an effective capture volume V. As the density N of activator ions is increased, the total capture volume corresponds to an effective activator density $n = N/(1+NV/2) \propto dL/d\mathcal{E}$. The less than linear increase of n with N is due to random overlap of individual ion capture volumes. Fitting this function to the data, one obtains $V \approx 1.2 \times 10^6$ Å^3, giving a capture radius of ~ 66 Å.

IV. MODEL OF SCINTILLATION

Although several models have previously been proposed to explain inorganic scintillation behavior,[20,34–37,39,45] none have combined all the following elements which we believe are crucial to account for alkali halide response to relativistic highly charged ions: (a) a calculation of the prompt dose profile, or "instantaneous" energy dose $g(r)$, r being the radial distance from the projectile trajectory; (b) allowance for the e-h pairs to migrate away from regions of high pair density and low scintillation efficiency; (c) use of a second-order quenching interaction. We combine these elements in the following way: the prompt ($t \approx 0$) energy dose $g(r)$ generated by an ion of charge Z_1 and energy E is calculated which includes the effect of δ-ray transport (see Appendix or Ref. 15 for details). Assuming 20 eV is required on the average to produce an e-h pair, the pair density $n(r)$ is then $\propto g(r)$. Next, in brief, $n(r,t=0)$ supplies the boundary for the kinetics equation $\partial n/\partial t = D\nabla^2 n - Kn^2$, which allows for simultaneous diffusion and self-annihilation of the e-h pairs. Evolution is computationally continued until $t = 10^{-8}$ sec, corresponding to the observed exciton (or e-h pair) lifetime in pure, room-temperature NaI of 15 nsec.[29] At that point all remaining pairs are assumed to migrate to activator (Tl^+) centers and contribute to luminescence; the scintillation efficiency is then the ratio of the total surviving number of luminescing pairs to the total initial ($t=0$) number of pairs. The numerical results to this model justify a posteriori our denial of the activator depletion hypothesis: the surviving (luminescent) pair density is less than the inverse of the Tl^+ capture volume previously calculated.

We now discuss our model in more detail. A typical dose curve is shown in Fig. 9. The very high densities calculated for very small r have meaning only in the trajectory direction; radially the dose falls off rap-

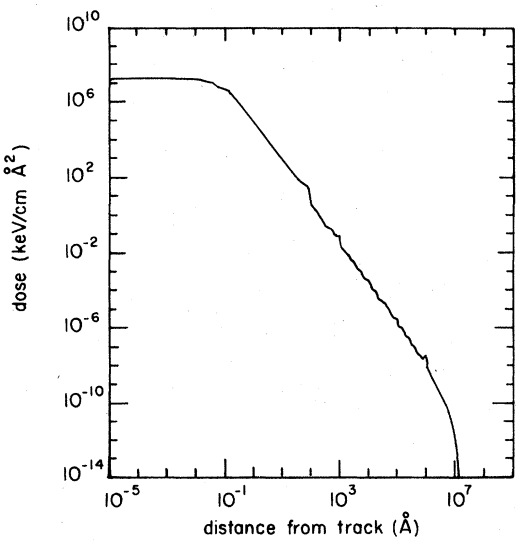

FIG. 9. Typical dose profile calculated by model for $Z=26$, $E=500$ MeV/amu. Both axes are logarithmic, dose units in the figure being keV/cm Å^2. The small peak at $\approx 10^6$ Å is due to absorption of iodine K-shell x rays at the photon absorption length. The general graininess in the "halo" region (where dose is due to δ-ray slowing) is an artifact of the finite-sized annuli.

idly, and over a distance comparable to the exciton size (a few Å) the average dose is much smaller. Calculation of second-order (n^2) processes using these high densities would yield an unphysically high degree of interaction. Instead, the densities at small radii were allowed to homogenize via diffusion until the axial separation between excitons became equal to the radial width of the homogenized dose (≥ 3 Å). Only then were other interactions turned on.

At this time, before further temporal evolution occurred, the exciton population was reduced via a process that is mathematically identical to the quenching factor of Katz and Kobetich[35] and of Ladu *et al.*,[36] although of different physical origin. Katz and Kobetich[35] resurrected the activator depletion hypothesis by assuming that sensitization (excitation) of an activator site obeys a cumulative one-or-more-hit Poisson distribution, so that the probability for sensitization of a given activator ion in a region of local energy density g is $P=1-\exp(-g/g_0)$ where g_0 is a dose parameter. The dose profile $g(r)$ (r is the radial distance from the ion trajectory) was calculated using the differential energy production cross section for δ rays only.[46] Their results overall match the experimental data of Newman and Steigert[1] (NS); this is due in part to their careful attention to a dose profile calculation. For those few ions where theory and experiment do not meet, an extension of the Katz and Kobetich model by Ladu *et al.*[36] provides a better fit. However, the Katz and Kobetich model predicts a decrease in heavy ion $dL/d\mathcal{E}$ for lower $d\mathcal{E}/dx$, $\sim 5\times10^2$–5×10^3 MeV cm^2/g, in contradiction to our experimental results. In our model, "prompt" *e-h* pair density reduction occurs because a single NaI molecule can accommodate only a limited number of *e-h* pairs (or exciton). If the *e-h* pair density exceeds this limit, the excess is presumed to be promptly quenched in some (unknown) manner. Given M sites for m particles, with the probability of a given site receiving a given particle being $1/M$, the mean number of occupied sites is $M[1-\exp(-m/M)]$, giving each *e-h* pair a survival probability of $[1-\exp(-m/M)]$, where m is proportional to the local dose g. If we were to postulate no further kinetic evolution, with all extant *e-h* pairs contributing to luminescence, our results would be identical to Katz and Kobetich's (apart from those dose calculation) upon equation of M with their characteristic dose g_0 (although their derivation employs the activator depletion hypothesis whereas ours does not). This sudden, *one-time e-h* pair loss contributed from 0% to 40% to the total quenching depending upon ion charge and velocity.

Further *e-h* pair loss resulted only from bimolecular annihilation as continued evolution obeyed the kinetics equation $\partial n/\partial t = D\nabla^2 n - Kn^2$. Integration was continued up to $t=10^{-8}$ sec, corresponding to the *e-h* pair lifetime, and ratios of remnant total energy to initial total energy were computed and equated to scintillation efficiency $dL/d\mathcal{E}$. Because of the high computational cost of doing so, loss terms in the dose differential equations corresponding to capture at activator sites and decay within the lattice were not included. Instead, the *e-h* pair decay was approximated at a step function as $t=10^{-8}$ sec.

The three parameters in our model are the *e-h* pair diffusion coefficient D, the second-order annihilation rate K, and the number of NaI molecules required to accommodate one *e-h* pair, η. Computational expense made impossible a thorough mapping of K-D-η space over a wide range of ion charges and energies. Instead, with η set to zero, the KD plane was searched and a locus determined ($K \propto D$) for which a 2.5-MeV α particle registered the experimentally observed degree of saturation. Then a complete set of $\{Z_1,E\}$ scintillation efficiency points were calculated for selected positions on the KD locus. Little variation in the resulting efficiency curves occurred over the KD locus, giving us the freedom to choose $D=10^{-4}$ cm^2/sec as being most consistent with experimental data,[47] thereby fixing K at 4×10^{-12} cm^3/sec. A small degree of fine tuning thereafter resulted in a choice of $\eta=2$.

In Fig. 10 the results of the model with these parameter values are compared to the proton and α data by Eby and Jentschke,[2] the heavy-ion data of Newman and Steigert,[1] and our relativistic heavy-ion data. Given the limited ability to optimize our fit by parameter variation, and given the crude step-function nature of our model's activator sensitization and exciton decay, the degree of fit over more than two orders of magnitude in $d\mathcal{E}/dx$ is impressive. Qualitatively, where not quantitatively, all experimentally observed features are reproduced. The degree of separation between the ^{20}Ne, ^{40}Ar, and ^{56}Fe efficiency curves closely follows our data. The α data also agree well with experiment. The proton points lie somewhat above the experimental values as a result of normalization of all calculated curves to allow matching of model and experiment at the 50 MeV/amu ^{20}Ne point. A slight degree of proton saturation is predicted by the model which very well may not have been detected by experiments in NaI, but which is strongly suggested by observation of proton saturation in CsI.[10] The poorest fits occur for the NS data, and even there the calculated efficiencies are not off by more than one charge unit. The most glaring deficiency is that the calculated low-energy heavy-ion slopes are not as steep as the NS data indicate. Part, though not all, of this discrepancy may be explained by noting that some of the stopping powers as calculated by NS for the lower of their measured heavy-ion energies are too low. Correcting for this would somewhat decrease the slopes of their experimental curves.

As discussed earlier, abrupt shifts in efficiency

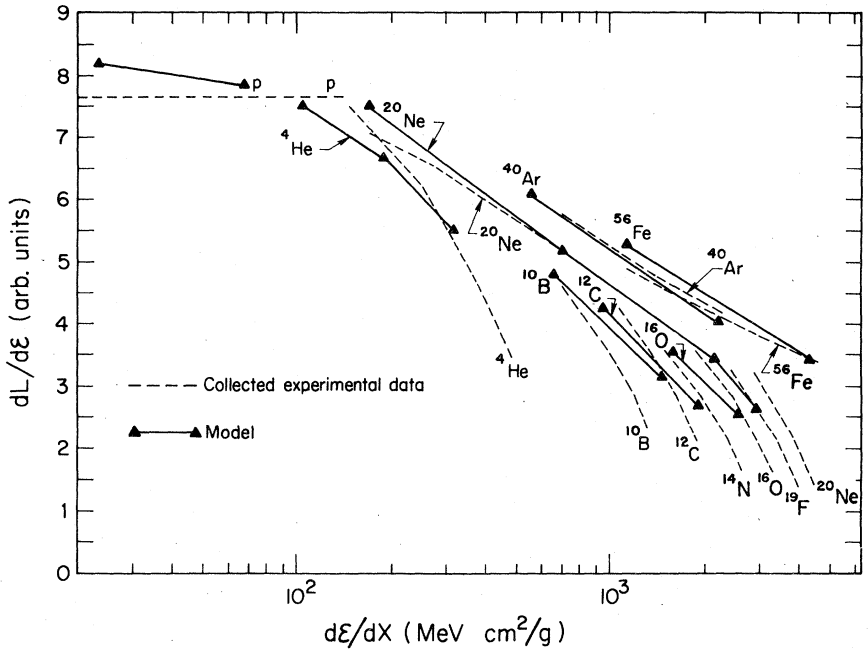

FIG. 10. Comparison of scintillation model with collected experimental data. Dashed lines give proton and α data of Ref. 2, the heavy-ion data of NS (Ref. 1), and our relativistic heavy-ion data. Triangles (Δ) mark scintillation efficiences calculated by the model; solid lines are drawn between them for ease of visualization only and are not to convey additional information.

curve slopes have been observed to occur at ~ 6 MeV/amu. The ^{20}Ne calculated curves shows such a slight shift at ~ 10 MeV/amu, as does the ^{4}He curve. We have not directly explored, however, the mechanism possible responsible for this observed shift.

One remarkable result of our model is an explanation for the absence of activator depletion as a mechanism contributing to saturation. As stated earlier, the absence of activator depletion implies an annihilation process so efficient that two e-h pairs cannot coexist for an e-h pair lifetime within the capture sphere of a Tl^+ ion. Our numerical results show that for *all* charges and energies, the maximum dose value just prior to activator sensitization at $t = 10^{-8}$ sec is always comparable to or less than the equivalent of one e-h pair per Tl^+ capture sphere volume. We emphasize that this is *not a priori* a necessary outcome of our model, although it does provide *a posterior* justification for our neglect of activator depletion as a saturation mechanism. That this upper limit on final dose ensues in an independent manner as a result of fitting calculated efficiency curves to data strengthens confidence in the underlying basis of this model.

We stress that the striking qualitative match between model and experiment over two orders of magnitude of $d\mathcal{E}/dx$ and for charges of $Z_1 = 1$ to 26 has not arisen from a careful selection of our three charge and energy-independent parameters. The qualtiative features shown in Fig. 10 are difficult to avoid with this model, which is fortuitous, since even a modest sensitivity of global efficiency behavior to the chosen parameters would have made it difficult, if not impossible, to converge on a reasonable fit given computational limitations. This characteristic of the model, along with its independent internal consistency with regard to activator depletion, supports the validity of its elements.

ACKNOWLEDGMENTS

We would like to thank Professor R. B. Murray for his very generous and informative discussions which occurred over the course of this work; they have substantially contributed to this paper. We also wish to thank Professor M. Luntz, Professor A. Portis, Professor F. Reif, and Dr. C. J. Delbecq and Dr. R. G. Kaufman for helpful conversations. We thank Professor P. B. Price for his continued support, and for this critical reading of the manuscript. We also thank the LBL Biomed research group for the kind use of their accelerator facilities. This work was supported by the Director, Office of Energy Research, Division of Nuclear Physics of the Office of High Energy and Nuclear Physics, Division of the U.S. Department of Energy under Contract No. W-7405-ENG-48.

APPENDIX: THE DOSE PROFILE

In our computer computation, the dose (histogram) profile is calculated by evaluating the energy deposited in annuli about the ion trajectory. The boundaries of the annuli are evenly spaced logarithmically from $R=10^{-5}$ Å to 10^{+8} Å, with 10 annuli per decade in radius. A very small lower limit is required to obtain close collisions with energy transfers near the kinematic limit, and the large upper limit corresponds to the range of the maximum energy δ ray produced for the ion energies under consideration.

The contribution to the total dose profile from each electron shell of the NaI molecule is calculated separately, using the ionization potentials I_i and oscillator strengths f_i given by Sternheimer[48] (see Table I). The electron shells are divided into two classes: "local" shells, in which the electronic energy of a barely ionized shell remains in the region occupied by the excited molecule, and "nonlocal" shells, in which subsequent Auger emission or x-ray fluorescence transports a significant fraction of the ionization potential energy away from its point of origin.

In both classes of shells, a close collision with the ion results in a high-energy δ ray of energy $\omega=\mathcal{E}-I$ where $\mathcal{E}$ is now defined as the total energy transferred during the collision and I is the ionization potential of the shell. Electron ejection perpendicular to the ion trajectory is assumed, an excellent approximation for all but the highest energies. Energy deposition in the crystal by slowing δ rays is calculated using an empirical electron range energy relation $r(\omega)=236\omega^{1.5}$ Å (ω in keV) determined from data of Katz and Penfold[49] and transmission functions of Rao.[50]

TABLE I. Shell parameters. For each principal atomic shell in the NaI molecular the average ionization potential I_i, oscillator strength $f_i(\sum_i f_i=1)$, and Ω_i are listed. Ω_i is the fraction of shell ionization energy not transported away from the molecule by Auger or fluorescence processes.

Shell	I_i (keV)	f_i	Ω_i
Na,K	1.07	$\frac{2}{64}$	0.10
Na,L	0.054	$\frac{8}{64}$	1.0
Na,M	0.005	$\frac{1}{64}$	1.0
I,K	33.2	$\frac{2}{64}$	0.023
I,L	4.79	$\frac{8}{64}$	0.08
I,M	0.766	$\frac{18}{64}$	0.24
I,N	0.091	$\frac{18}{64}$	1.0
I,O	0.027	$\frac{7}{64}$	1.0

The primary energy transferred to a shell electron during a collision is calculated using the results of Bohr[51] who found the energy transfer to a harmonically bound electron of frequency $I/\hbar$ by a passing ion of charge Z_1, velocity βc, and impact parameter b to be

$$\mathcal{E}(b)=\frac{2Z_1^2e^4}{m_ec^2\beta^2b^2}\left[\xi^2K_1^2(\xi)+\frac{\xi^2K_0^2(\xi)}{\gamma^2}\right],$$

where $m=e^-$ mass, $\xi\equiv(Ib/\hbar c\beta\gamma)$, $\gamma=(1-\beta^2)^{-1/2}$, and $K_0(\xi)$, $K_1(\xi)$ are modified Bessel functions. Ahlen[17] has advanced arguments for the continued validity of the above expression down to impact parameters well within the atomic volume, in fact down to $b^q_{\min}=\hbar/\gamma mc\beta$ when $Z_1\alpha/\beta<1$, where $\alpha=e^2/\hbar c$, and $b^q_{\min}$, being the wavelength of the scattered electron, represents the smallest impact parameter meaningful in a classical sense. At extremely small "impact parameters," $\mathcal{E}(b)$ approaches asymptotically $E_{\max}=2mc^2\beta^2\gamma^2$, the kinematic limit to energy transfer. To join the Bohr expression, $\propto 1/b^2$, to the constant, maximum energy transfer value, an intermediate curve segment $\propto 1/b$ is inserted at points b_1 (connecting to $E_{\max}$) and b_2 (connecting to the Bohr formula) to give a single expression for energy transfer.

$$\mathcal{E}(b)=\mathcal{E}_{\max}\left[\frac{b_1}{b+b_1}\right]\left[\frac{b_2}{b+b_2}\right]\left[\xi^2K_1^2(\xi)+\frac{\xi^2K_0^2(\xi)}{\gamma^2}\right],$$

where

$$b_1b_2=\left[\frac{Z_1e^2}{\gamma mc^2\beta^2}\right]^2.$$

The parameter b_2 (and hence b_1) is determined by requiring the sum of $\mathcal{E}(b)$ over all electrons to be equal to total stopping power as given by the Bethe-Bloch formula.[17]

Using this expression, the mean energy transfer $\mathcal{E}$ to a given shell electron at the sampling coordinate of an annulus is calculated. If $\mathcal{E}>I$, every shell electron in the annulus is excited and propagates outward as a δ ray of energy $\omega=\mathcal{E}-I$. If $\mathcal{E}<I$, then ionization is assumed to occur in the fraction $(\mathcal{E}/I)$ of electrons, the remainder being unexcited. The ionized electrons in this case are assumed to have energy $\omega=0$ (although integration over low-velocity ionization cross sections[52] gives a mean electron energy of up to $\omega=0.12I$).

Excited inner shells decay either through Auger electron emission or through x-ray fluorescence, with x-ray fluorescence being significant only for iodine K shell (88%). Ionization of the iodine L shell, for ex-

ample, is followed by Auger emission leaving two M-shell vacancies; these are followed by $N \rightarrow M$ Auger transitions, etc., until only shells of ionization potential <0.1 keV are left empty, these being assumed not to contribute to further energy transport. As an approximation to isotropic emission, Auger electrons are emitted at 45° in our model. Table I gives the fraction Ω of initial ionization potential energy left behind in each shell after these processes. $\Omega < 1$ for "nonlocal" shells and $\Omega = 1$ for "local" shells. Figure 9 shows a typical dose profile calculated with this model.

---

*Present address: Dept. of Physics, University of Utah Salt Lake City, Utah 84112.

[1]E. Newman and F. E. Steigert, Phys. Rev. 118, 1575 (1960).
[2]F. S. Eby and W. K. Jentschke, Phys. Rev. 96, 911 (1954).
[3]J. W. Blue and D. C. Liu, I. R. E. Trans. Nucl. Sci. 9, 48 (1962).
[4]S. K. Allison and H. Casson, Phys. Rev. 90, 880 (1953).
[5]M. R. Altman, H. B. Dietrich, R. B. Murray, and T. J. Rock, Phys. Rev. B 7, 1743 (1973).
[6]R. W. Birkmire, R. B. Murray, and M. Luntz, Phys. Rev. B 15, 31 (1977).
[7]J. C. D. Milton and J. S. Fraser, Phys. Rev. 96, 1508 (1954).
[8]E. N. Shipley, G. E. Owen, and L. Madansky, Rev. Sci. Instrum. 30, 604 (1959).
[9]R. H. Lovberg, Phys. Rev. 84, 852 (1951).
[10]R. Gwin and R. B. Murray, Phys. Rev. 131, 501 (1963).
[11]E. A. Womack, A. J. Lazarus, and S. W. W. Liu, Phys. Rev. 144, 231 (1966).
[12]J. B. Schutt, J. F. Arens, C. M. Shai, and E. Stromberg, Appl. Opt. 13, 2218 (1974).
[13]S. P. Ahlen, B. G. Cartwright, and G. Tarlé, Nucl. Instrum. Methods 143, 513 (1977).
[14]M. H. Salamon and G. Tarlé, Nucl. Instrum. Methods 161, 147 (1979).
[15]M. H. Salamon and S. P. Ahlen , Lawrence Berkeley Laboratory Report No. 12269 (unpublished).
[16]M. H. Salamon, Lawrence Berkeley Laboratory Report No. 10466 (unpublished).
[17]S. P. Ahlen, Rev. Mod. Phys. 52, 121 (1980).
[18]M. H. Salamon, S. P. Ahlen, G. Tarlé, and K. C. Crebbin, Phys. Rev. A 23, 73 (1981).
[19]A. R. Quinton, C. E. Anderson, and W. J. Knox, Phys. Rev. 115, 886 (1959).
[20]J. B. Birks, *The Theory and Practice of Scintillation Counting* (Pergamon, New York, 1964).
[21]R. G. Kaufman, W. B. Handley, and H. N. Hersh, IEEE Trans. Nucl. Sci. 17, 82 (1970).
[22]R. B. Murray, IEEE Trans. Nucl. Sci. 22, 54 (1975).
[23]H. B. Dietrich, A. E. Purdy, R. B. Murray, and R. T. Williams, Phys. Rev. B 8, 5894 (1973).
[24]W. B. Hadley, S. Polick, R. G. Kaufman, and H. N. Herse, J. Chem. Phys. 45, 2040 (1966).
[25]R. T. Williams, J. N. Bradford, and W. L. Faust, Phys. Rev. B 18, 7038 (1978).
[26]T. G. Castner and W. Känzig, J. Phys. Chem. Solids 3, 178 (1957).
[27]R. D. Popp and R. B. Murray, J. Phys. Chem. Solids 33, 601 (1972).
[28]See, e.g., *Radiationless Processes in Molecules and Condensed Phases,* edited by F. K. Fong (Springer, Berlin, 1976).
[29]W. J. Van Sciver and L. Bogart, I. R. E. Trans. Nucl. Sci. N2-3, 90 (1958).
[30]C. J. Delbecq, A. K. Ghosh, and P. H. Yuster, Phys. Rev. 151, 599 (1966).
[31]C. J. Delbecq, Y. Toyozawa, and P. H. Yuster, Phys. Rev. B 9, 4497 (1974).
[32]H. B. Dietrich and R. B. Murray, J. Lumin. 5, 155 (1972).
[33]I. K. Pliavin', Opt. Spectrosc. 7, 41 (1959).
[34]R. B. Murray and A. Meyer, Phys. Rev. 122, 815 (1961).
[35]R. Katz and E. J. Kobetich, Phys. Rev. 170, 397 (1968).
[36]M. Ladu, M. Pellicioni, and M. Roccella, Nucl. Instrum. Methods 101, 383 (1972).
[37]J. B. Birks, IEEE Trans. Nucl. Sci. NS-11, 4 (1964).
[38]R. Voltz, J. Lopes da Silva, G. Laustriat, and A. Coche, J. Chem. Phys. 45, 3306 (1966).
[39]M. Luntz, Phys. Rev. B 4, 2857 (1971).
[40]R. C. Powell and L. A. Harrah, J. Chem. Phys. 55, 1878 (1971).
[41]N. A. Tolstoi and A. P. Abramov, Opt. Spectrosc. 20, 273 (1966).
[42]E. Strauss, W. J. Maniscalco, W. M. Yen, U. C. Kellner, and V. Gerhardt, Phys. Rev. Lett. 44, 824 (1980).
[43]J. A. Harshaw, H. C. Kremers, E. C. Stewart, E. K. Warburton, and J. O. Hay, U.S. AEC Report NY0-1577 (unpublished). See Ref. 34 for display of this data.
[44]P. D. Johnson and F. E. Williams, J. Chem. Phys. 18, 1477 (1950).
[45]A. Meyer and R. B. Murray, Phys. Rev. 128, 98 (1962).
[46]E. J. Kobetich and R. Katz, Phys. Rev. 170, 391 (1968).
[47]H. Nishimura and M. Tomura, J. Phys. Soc. Jpn. 39, 390 (1975).
[48]R. M. Sternheimer, Phys. Rev. 164, 349 (1967).
[49]L. Katz and A. S. Penfold, Rev. Mod. Phys. 24, 28 (1952).
[50]B. N. S. Rao, Nucl. Instrum. Methods 44, 155 (1966).
[51]N. Bohr, Philos. Mag. 25, 10 (1913); 30, 581 (1915).
[52]E. Merzbacher and H. W. Lewis, *Encyclopeida of Physics* (Springer, Berlin, 1958), Vol. 34/2, p. 166.